Journal of Organometallic Chemistry 879 (2019) 144–149

Contents lists available at ScienceDirect

Journal of Organometallic Chemistry

journal homepage: www.elsevier.com/locate/jorganchem

A platinum(II)-acetylide-based conjugated polyelectrolyte for hypoxia imaging via ratiometric and time-resolved luminescence microscopy

Guo Li, Tianci Huang, Mingjuan Xie, Xiangxiang Zhang, Qi Yu, Shujuan Liu**, Tianshe Yang, Qiang Zhao*

Key Laboratory for Organic Electronics and Information Displays & Jiangsu Key Laboratory for Biosensors, Institute of Advanced Materials (IAM), Nanjing University of Posts and Telecommunications (NUPT), 9 Wenyuan Road, Nanjing 210023, China

ARTICLE INFO

Article history:
Received 31 August 2018
Received in revised form
15 October 2018
Accepted 18 October 2018
Available online 22 October 2018

Keywords:
Hypoxia
Conjugated polyelectrolyte
Pt(II) complex
Ratiometric imaging
Time-resolved photoluminescence imaging

ABSTRACT

A platinum(II)-acetylide-based conjugated polyelectrolyte has been designed and synthesized by using polyfluorenes as an O_2-insensitive fluorophore and Pt(II) complex as an O_2-sensitive phosphor, which can generate conjugated polyelectrolyte nanoparticle (CPE-nanoparticle) in the aqueous solution owing to their amphiphilic structures. The CPE-nanoparticle displays good sensitivity to O_2 concentration and can detect oxygen levels reversibly. The intracellular ratiometric O_2 sensing performance of the CPE-nanoparticle has been demonstrated by the remarkable variation in the I_{green}/I_{blue} ratio values (0.18–0.85) in HeLa cells under different O_2 levels. Furthermore, O_2 level detection was carried out through time-resolved luminescence imaging (TRLI) to demonstrate the accuracy of the probe based on the CPE-nanoparticle. The CPE-nanoparticle shows a high phosphorescence quantum yield (19.98%) and oxygen quenching efficiency (0.975), which are superior to the existing O_2 probe. The CPE-nanoparticle has been successfully applied in photoluminescence lifetime imaging and time-gated luminescence imaging for monitoring intracellular O_2 levels.

1. Introduction

Cellular oxygen (O_2), which plays a crucial role in many physiological process, is one of the most vital components in biological systems [1]. Hypoxia, defined as oxygen-deprived condition, is a distinct feature of multifarious disease including tumors [2], stroke [3], and retinal disease [4]. In some solid tumors, the median oxygen concentration has been reported to be around 4%, and locally, it can be as low as 0% [5]. Therefore, accurate detection of tumor hypoxia is not only great importance for disease diagnosis, but also can be used to evaluate therapeutic effects. Therefore, attention has been dedicated to the development of hypoxia probe.

To date, immunostaining [6–8], magnetic resonance imaging [9,10], positron emission tomography imaging [11–13], near infrared tomographic imaging [14,15] and optical imaging [16,17] are available approaches to detect hypoxic regions *in vitro* and *in vivo*. As a non-invasive optical technology, optical imaging has been an outstanding method to map oxygen in biological samples owing to the high sensitivity and spatial resolution [18,19]. However, extremely low intracellular oxygen level and long incubation time may be required for most of these probes [20–22]. Moreover, the binding of these probes to cancer cells is also obviously impaired by the low pH of the tumor microenvironment [23,24]. All the limitations compromise the application of these probes in accurately detection hypoxia in cancer cells and tumor tissues.

Phosphorescent transition metal complexes (PTMCs), which possess long lifetime, can be used as an effective probe in imaging to eliminate short-lived autofluorescence and increase the signal-to-noise ratio by time-resolved photoluminescence technique (TRPT) [25,26]. Additionally, PTMCs own distinctive advantages that are suitable to be used as bio-probes, including the tunable emission, good cell membrane permeability and high quantum yields. The triplet excited state of PTMCs is usually responsive to the triplet ground state of molecular oxygen through energy transfer [27,28]. PTMCs have attracted considerable interest in imaging and sensing the oxygen level *in vitro* and *in vivo* [29–34]. However, most of these oxygen probes are usually water insoluble and based on the single variation of phosphorescent emissive intensity, which is easily influenced by the complex intracellular microenvironment and external experimental conditions, such as excitation power and

* Corresponding author.
** Corresponding author.
E-mail addresses: iamsjliu@njupt.edu.cn (S. Liu), iamqzhao@njupt.edu.cn (Q. Zhao).

https://doi.org/10.1016/j.jorganchem.2018.10.014
0022-328X/

probe concentration. Therefore, ratiometric probes, whose ratio represents the variation value of the emission intensities at two paths, can improve the accuracy for hypoxia sensing [32,35], as well as eliminate photobleaching and excitation power fluctuation [36]. In addition, many polyfluorene based and Pt-porphyrin based O_2 probes have shown high reliability and full reversibility for measuring oxygen concentrations [32,37,38].

Conjugated polyelectrolytes (CPEs) is a good choice, owing to their distinguished merits such as strong absorbance, easy modification, high fluorescent efficiency, good photostability and biocompatibility [39–43]. In addition, the charged side chains of CPEs allow them good solubility in aqueous solution, which is beneficial for bioimaging and biosensing *in vitro* and *in vivo* [44,45].

Considering the merits of both PTMCs and CPEs, herein, a dual-emissive conjugated polyelectrolytes containing platinum acetylide has been designed and synthesized for hypoxia sensing. A long-lived phosphorescent platinum(II) complex has been introduced into conjugated polyelectrolyte as the O_2-sensitive phosphorescent moieties, and O_2-insensitive fluorescence from polyfluorene moieties as a reference. Therefore, the dual-emissive CPE-nanoparticle has been successfully synthesized as O_2 probes. The ratiometric measurements of hypoxia were carried out in living cells. In addition, O_2 levels in living cells have been investigated through time-resolved luminescence imaging techniques, including photoluminescence lifetime imaging microscopy (PLIM) and time-gated luminescence imaging (TGLI). These results indicated that CPE-nanoparticle is ideal luminescent probes in monitoring O_2 concentrations in living biological samples.

2. Experimental section

All materials and regents were used as received from commercial sources unless stated otherwise. The solvents (NEt_3 and CH_2Cl_2) were purified under reflux over CaH_2 for several hours, distilled at these conditions. The structure of **P1** was characterized by ^{1}H NMR and gel permeation chromatography (GPC). Transmission electron microscopy (TEM) was conducted on a JEOL transmission electron microscope (JEM-2100). Average particle size was measured by dynamic light scattering (DLS) on Zetasizer Nanoseries (Nano ZS90). Zeta-potential was measured by Zeta-plus zeta potential analyzer. The UV–visible absorption spectra were recorded using a Shimadzu UV-3600 UV-VIS-NIR spectrophotometer. Oxygen concentration was monitored by Mass Flow Controller or oxygen concentration-changeable multigas incubator during the spectra, lifetime and cell imaging measurements.

The conjugated polyelectrolyte **P1** was obtained in the presence of catalytic amount of CuI via reaction between *trans*-$PtCl_2(PBu_3)_2$ and the diethynyl ligand (Scheme 1). **M1** (302 mg, 0.50 mmol), **Pt1** (335 mg, 0.50 mmol) and CuI (9.5 mg, 0.05 mmol) in distilled 40 mL Et_3N/CH_2Cl_2 (1:1, v/v) were stirred for 0.5 h at room temperature under nitrogen. After the reaction was finished, the solvent was evaporated under reduced pressure. After concentrating the CH_2Cl_2 solution, yellow solid was collected by precipitation into a large excess of methanol. Condensed trimethylamine (3 mL) was added dropwise to a solution of the polymer **P1** (150 mg) in THF (20 mL) at −78 °C using dry ice-acetone bath. The mixture was stirred for 24 h at room temperature. After removing most of the solvent, acetone was added to precipitate **P2**. The resulting polymers were dried under vacuum with a yield of 65%.

3. Results and discussion

3.1. Synthesis and characterization

To develop a new and excellent dual-emissive long-lived hypoxia probes for biosensing and bioimaging, Pt coordination centers is directly introduced onto the fluorene π-conjugated backbones. The synthetic routes and the chemical structures of the CPEs were illustrated in Scheme 1 and Scheme S1 in the Supporting Information (SI). The platinum acetylide-based polymer **P1** containing fluorene unit was obtained in the presence of CuI as catalyst via reaction between *trans*-$PtCl_2(PBu_3)_2$ and the diethynyl ligand. The structure of **P1** was characterized by ^{1}H NMR. The molecular weight of conjugated polyeletrolyte was characterized by GPC ($M_n \approx 54\,724$ and $M_w \approx 96\,596$ with polydisperisity index PDI = 1.76). The target platinum acetylide-based polyelectrolyte **P2** was prepared via the quarternization of the precursor **P1**.

To investigate the size and morphology of **P2,** TEM and DLS measurements were carried out and the results were shown in Fig. 1a and Fig. S2. The size of CPE-nanoparticle was about 3 nm, which was formed through self-assembly, owing to the amphiphilic structures of **P2** with hydrophobic backbones and hydrophilic side chains. As show in Fig. S2b, DLS measurement shows that CPE-nanoparticle possessed an average hydrodynamic diameter of about 12 nm, which is larger than that measured by TEM because of the shrinkage at dry state on copper grid. In addition, the results of zeta-potential was 31.00 mV, facilitating the interaction with cell membrane potential through electrostatic interactions.

3.2. Photophysical properties

The photophysical properties of **P2** have been investigated by UV–vis absorption and luminescence spectra. As shown in the absorption spectrum of Fig. 1b, the absorption peak of **P2** centers at 396 nm in aqueous solution, and the molar absorption coefficients of CPE-nanoparticle is 4856 $g^{-1}cm^{-1}$, which is ascribed to the π-π* transition of the fluorene-based platinum acetylide backbone (Fig. 1b). In the emission spectra of **P2**, two major emission bands at 415 and 550 nm were observed in degassed aqueous solution, which were assigned to polyfluorene main chain and Pt(II) complex, respectively. The high-energy band of the emission spectra is attributed to the fluorescence emission from ^{1}π-π* state of fluorene with short lifetime ($\tau_F = 0.33$ ns), while the emission band at 550 nm is from the long-lived phosphorescence from Pt complex ($\tau_P = 5.96$ μs). The phosphorescence quantum yield of CPE-nanoparticle under N_2 is 19.98%, which is higher than the previous reports about Ru(II) and Ir(III) complexes [31,46]. Moreover, **P2** show no Förster resonance energy transfer (FRET) between the polyfluorenes and Pt(II) complex according to the excitation spectra (Fig. S3).

3.3. Luminescence response to O_2 content

To investigate the oxygen-responsive ability of **P2**, the emission spectra of the CPE-nanoparticle under different oxygen concentrations in aqueous solution were measured, and the results were shown in Fig. 1c. Under 159.6 mmHg O_2, the emissions at 415 nm and 430 nm of CPE-nanoparticle, which was attributed to polyfluorene units, were stronger than those at 550 nm and 590 nm from Pt(II) complex. When the O_2 level decreased, the intensity of fluorescence at 415 nm showed negligible change, while the green emission intensity at 550 nm enhanced remarkably, revealing the phosphorescence sensitivity of Pt(II) complex to O_2. Therefore, a ratiometric oxygen probe was achieved in aqueous solution based on the phosphorescent CPE-nanoparticle.

The quantitative oxygen sensing performance of the CPE-nanoparticle was investigated through the emission as shown in Fig. 1c. The oxygen level can be calculated according to the Stern-Volmer equation:

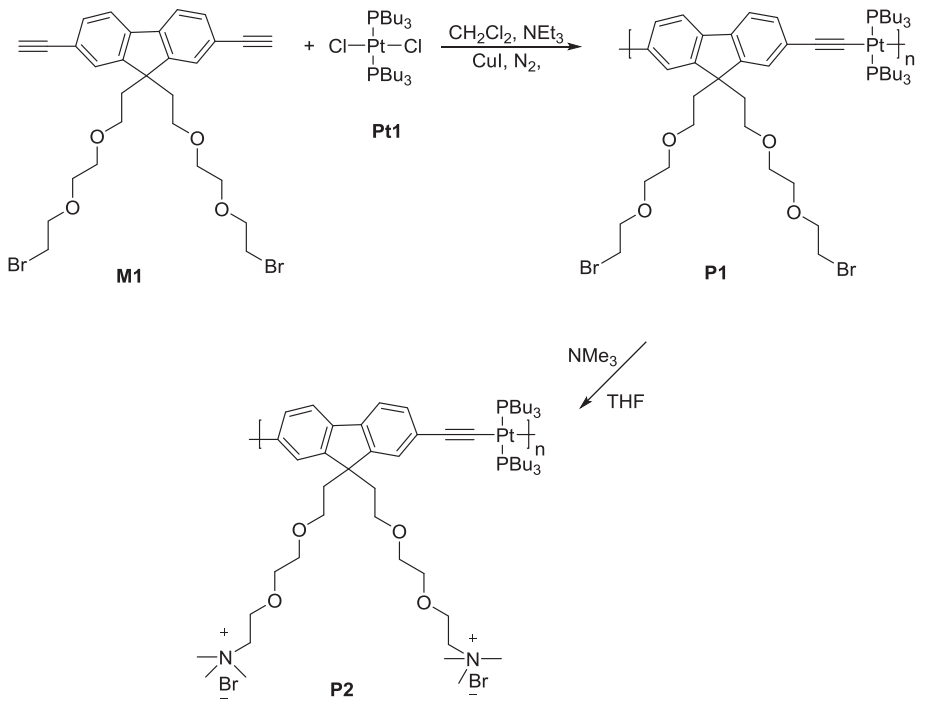

Scheme 1. Synthetic route of the target conjugated polyelectrolyte **P2** and the intermediate **P1**.

$$\frac{R_I^0}{R_I} = 1 + K_{SV} pO_2 \quad (1)$$

where K_{sv} is the constant of quenching rate, pO_2 is the oxygen level, $R_I{}^0 = (I^0_{550}/I^0_{415})$ and $R_I = (I_{550}/I_{415})$ are the ratios of the phosphorescence (550 nm) intensity of Pt(II) complex to the fluorescence (415 nm) intensity of the polyfluorene units in the absence and presence of O_2, respectively.

As shown in Fig. 1d and Fig. S4, $R_I{}^0/R_I$ and pO_2 revealed a good linear relationship and the K_{sv} value is calculated to be 1.17×10^{-2} mmHg^{-1}. Moreover, small fluctuation was found at 415 nm under different O_2 concentrations (Fig. 1c), demonstrating that the ratio of the emissive intensity at 550 nm and at 415 nm of the CPE-nanoparticle relied on O_2 level. Thus, the O_2 concentration can be calculated based on the value of K_{sv}.

To demonstrate the oxygen quenching efficiency, the emission spectra of CPE-nanoparticle in aqueous solution saturated with N_2 and O_2 were measured (Fig. S4a). According to the following equation:

$$Q = (R_{N_2} - R_{O_2})/R_{N_2}$$

where Q is the oxygen quenching efficiency, and R_{N2} and R_{O2} are the emission intensity ratios between phosphorescence at 550 nm and fluorescence at 415 nm for the CPE-nanoparticle solution saturated with N_2 and O_2, the Q value was estimated to be 0.975, suggesting high sensitivity of CPE-nanoparticle for oxygen as compared with previous report [33].

3.4. Lifetime response to O_2

In addition, the O_2 sensing was also investigated by lifetime measurements. The oxygen level can be calculated according to the Stern-Volmer equation:

$$\frac{\tau_0}{\tau} = 1 + K_{SV} O_2 \quad (2)$$

where K_{sv} is the quenching constant, pO_2 is the oxygen level, τ_0 and τ are the phosphorescence lifetimes in the absence and presence of O_2, respectively.

As shown in Fig. 1e, the luminescence lifetime at 550 nm of CPE-nanoparticle in degassed conditions was 30.52 μs. The lifetime decreased to 5.96 μs when the O_2 level enhanced to 159.6 mmHg. In addition, τ_0/τ and pO_2 had a good linear relationship, as shown in Fig. 1f. According to the slope of the trend line, the K_{sv} value is calculated to be 2.71×10^{-2} mmHg^{-1}. However, the fluorescence lifetime at 415 nm of the CPE-nanoparticle remains unchanged at different O_2 levels (Fig. S5). As a result, the CPE-nanoparticle can be used as a hypoxia probe through luminescence lifetime measurements.

3.5. Cell cytotoxicity

To evaluate the cytotoxicity of the CPE-nanoparticle in living cells, MTT (methyl thiazolyl tetrazolium) assay was carried out for CPE-nanoparticle under different concentration (Fig. S6). The result of cell viabilities (%) versus incubation concentrations (0–100 μg mL^{-1}) of the CPE-nanoparticle in PBS buffer at 37 °C for 72 h is elucidated in Fig. S6. The cell viability was more than 78% when CPE-nanoparticle (100 μg mL^{-1}) was added in the incubation medium for 72 h, demonstrating that the CPE-nanoparticle has low cytotoxicity and excellent biocompatibility for potential biological applications. Furthermore, we use flow cytometry assay to elaborate the toxicity of the CPE-nanoparticle. As shown in Fig. S7, cell apoptosis quantity was few, indicating that the CPE-nanoparticle has slight cell damage. Flow cytometry assay suggested that the probe toxicity was negligible.

3.6. Ratiometric measurement of hypoxia in vitro

To investigate the capability of hypoxia sensing quantitatively in

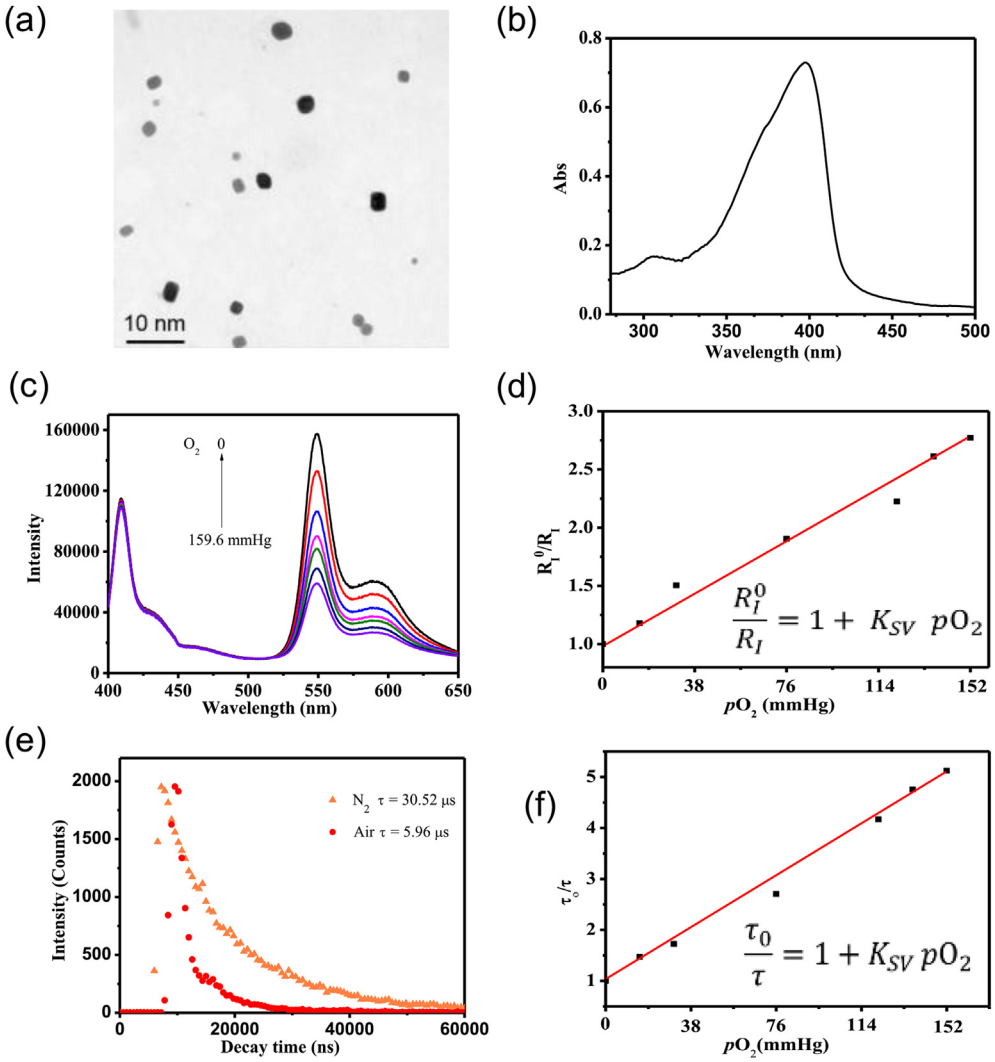

Fig. 1. (a) A TEM image of CPE-nanoparticle in aqueous solution. (b) Absorption spectrum of CPE-nanoparticle (15 μg mL^{-1}) in aqueous solution. (c) Emission spectra of CPE-nanoparticle (15 μg mL^{-1}) in aqueous solution under different O_2 concentrations excited at 365 nm. (d) Plot of R_I^0/R_I as a function of O_2 concentration. (e) Phosphorescence decays of CPE-nanoparticle in aqueous solution saturated with N_2 or air, monitored at 550 nm from the Pt(II) complex excited at 405 nm. (f) Plot of τ_0/τ as a function of O_2 concentration (λ_{ex} = 405 nm). All the measurement were acquired at room temperature.

living cells, ratiometric measurement was carried out by using CPE-nanoparticle. HeLa cells (human cervical carcinoma cells) were cultured at 37 °C with the CPE-nanoparticle in PBS at pH 7.4 under 159.6 mmHg, 76 mmHg, 38 mmHg and 19 mmHg oxygen levels for 4 h. Under excitation at 405 nm, the fluorescence and phosphorescence signals were collected at blue (410–460 nm) and green (520–580) channel, respectively.

As shown in Fig. 2 and Figs. S8–S9, the emission at the blue channel almost remained a certain value under different oxygen concentrations, while the phosphorescence emission from Pt(II) complex enhanced with decreasing oxygen level. The ratio of phosphorescence signal (I_{green}) to fluorescence signal (I_{blue}) also increased from 0.18 to 0.85 along with the decreasing of oxygen level from 159.6 mmHg to 19 mmHg, which allows us to monitor the concentration of oxygen.

3.7. TRLI images of intracellular O_2 concentration

Considering the phosphorescence lifetime of CPE-nanoparticle showed a good linear relationship with oxygen level, lifetime imaging was also conducted to monitor the intracellular oxygen level

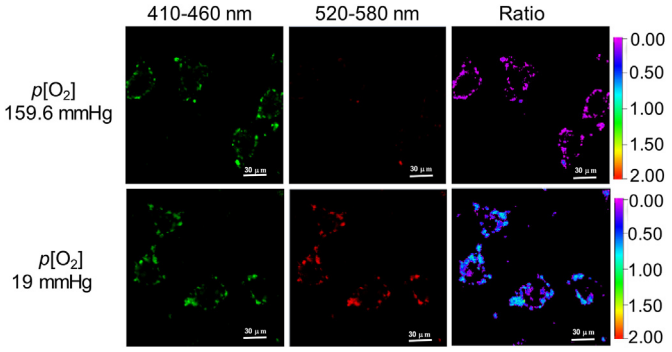

Fig. 2. Confocal luminescence imaging and ratiometric luminescence imaging (λ_{ex} = 405 nm) of Hela cells incubated with the polymer (20 μg mL^{-1}) at 159.6 mmHg or 19 mmHg O_2 concentrations. In luminescence imaging, the emission channels at wavelengths of 410–460 nm and 520–580 nm were collected, respectively. In ratiometric imaging, the ratio of emission intensity at 520–580 nm to that at 410–460 nm was chosen as the detected signal.

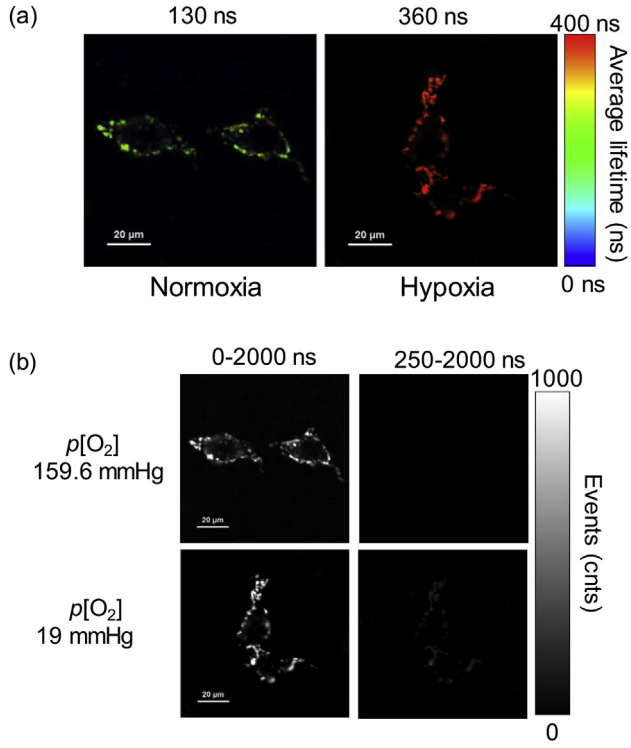

Fig. 3. (a) Photoluminescence lifetime images ($\lambda_{ex} = 405$ nm) of Hela cells incubated with the polymer (20 μg mL^{-1}) at 37 °C for 2 h at 159.6 mmHg and 19 mmHg O_2 concentrations, respectively. The magnification of the objective lens is 60 ×. The luminescence signals were collected in the range of 520–600 nm. (b) Time-gated luminescence intensity images ($\lambda_{ex} = 405$ nm) of Hela cells incubated with the polymer 20 μg mL^{-1} at 37 °C for 2 h at 159.6 mmHg or 19 mmHg O_2 concentrations with different time delays. The magnification of the objective lens is 60 ×. The luminescence signals were collected in the range of 410–580 nm.

by using CPE-nanoparticle as a lifetime-based probe. The mean emission lifetime τ was approximately 130 ns (159.6 mmHg) and 360 ns (19 mmHg), demonstrating the sensitive response of the lifetime of CPE-nanoparticle towards O_2 levels (Fig. 3a). The PLIM results indicated that the emission signals from CPE-nanoparticle could be distinguished from the interference of short-lived autofluorescence. Therefore, it is feasible to use the CPE-nanoparticle as a potential lifetime probe for discriminating normoxia and hypoxia in living cells.

Furthermore, to eliminate the short-lived autofluorescence in complicated conditions in living cells, TGLI imaging was used to monitor the intracellular oxygen level (Fig. 3b). Without delay time, the signals of images showed a similar intensity at 159.6 mmHg and 19 mmHg concentrations, owing to the reference fluorescence from short lifetime moieties. However, by exerting a 250 ns decay time, the signal of the images at 159.6 mmHg concentration disappeared whereas the signal of the images at 19 mmHg O_2 concentration was still observed, which ascribed to the long-lived phosphorescence from Pt(II) complex of the CPE-nanoparticle. These results indicated that hypoxia sensing could be more accurate by exerting a long delay time. Therefore, TGLI imaging can avoid anti-interference effectively on the basis of long-lived phosphorescence signal.

4. Conclusion

In summary, a dual emissive and biocompatible hypoxia probe CPE-nanoparticle has been developed for the high sensitive and reliable imaging of hypoxia. The phosphorescence emissive intensity and lifetime from CPE-nanoparticle showed an excellent sensitivity to oxygen level. The probe can be readily used for ratiometric measurement, allowing for the quantitative evaluation of the hypoxia concentration in living cells with low cytotoxicity. Furthermore, the CPE-nanoparticle can employ TRLI techniques to monitor O_2, which can remarkably improve the sensitivity and accuracy. We believe that the CPE-nanoparticle can provide a specific tool for hypoxia imaging, and will enrich the design of ratiometric and lifetime-based probes for monitoring hypoxia in living cells. Further work will focus on developing efficiently NIR-excitable hypoxia probes *in vivo*.

Acknowledgments

This work was supported by the National Natural Science Foundation of China (51473078, 21501098 and 21671108), National Program for Support of Top-Notch Young Professionals, Scientific and Technological Innovation Teams of Colleges and Universities in Jiangsu Province (TJ215006), and Priority Academic Program Development of Jiangsu Higher Education Institutions (YX03001).

Appendix A. Supplementary data

Supplementary data to this article can be found online at https://doi.org/10.1016/j.jorganchem.2018.10.014.

References

[1] J. Aragonés, P. Fraisl, M. Base, P. Carmeliet, Cell Metabol. 9 (2009) 11–22.
[2] W.R. Wilson, M.P. Hay, Nat. Rev. Canc. 11 (2011) 393–410.
[3] K. Prass, A. Scharff, K. Ruscher, D. Lowl, C. Muselmann, I. Victorov, K. Kapinya, U. Dirnagl, A. Meisel, Stroke 34 (2003) 1981–1986.
[4] R.N. Frank, N. Engl, J. Med. 350 (2004) 48–58.
[5] P. Vaupel, K. Schlenger, C. Knoop, M. Hockel, Cancer Res. 51 (1991) 3316–3322.
[6] S. Kizaka-Kondoh, M. Inoue, H. Harada, M. Hiraoka, Cancer Sci. 94 (2003) 1021–1028.
[7] A.L. Harris, Nat. Rev. Canc. 2 (2003) 38–47.
[8] E.K. Rofstad, H. Rasmussen, K. Galappathi, B. Mathiesen, K. Nilsen, B.A. Graff, Cancer Res. 62 (2002) 1847–1853.
[9] T. Inoue, E. Kozawa, H. Okada, K. Inukai, S. Watanabe, T. Kikuta, Y. Watanabe, T. Takenaka, S. Katayama, J. Tanaka, H. Suzuki, J. Am. Soc. Nephrol. 22 (2011) 1429–1434.
[10] S. Iwaki, K. Hanaoka, W. Piao, T. Komatsu, T. Ueno, T. Terai, T. Nagano, Bioorg. Med. Chem. Lett. 22 (2012) 2798–2802.
[11] S. Apisarnthanarax, K.S.C. Chao, Radiat. Res. 163 (2005) 1–25.
[12] J.L.J. Dearlin, J.S. Lewis, G.E.D. Mullen, M.J. Welch, P.J.J. Blower, Biol. Inorg. Chem. 7 (2002) 249–259.
[13] D.J. Yang, S. Wallace, A. Cherif, C. Li, M.B. Gretzer, E.E. Kim, D.A. Podoloff, Radiology 194 (1995) 795–800.
[14] B.M. Fenton, S.F. Paoni, J. Lee, C.J. Koch, E.M. Lord, Br. J. Canc. 79 (1999) 464–471.
[15] H.L. Liu, Y.L. Song, K.L. Worden, X. Jiang, A. Constantinescu, R.P. Mason, Appl. Opt. 39 (2000) 5231–5243.
[16] K. Kiyose, K. Hanaoka, D. Oushiki, T. Nakamura, M. Kajimura, M. Suematsu, H. Nishimatsu, T. Yamane, T. Terai, Y. Hirata, T. Nagano, J. Am. Chem. Soc. 132 (2010) 15846–15848.
[17] G.M. Palmer, A.N. Fontanella, S.Q. Shan, G. Hanna, G.Q. Zhang, C.L. Fraser, M.W. Dewhirst, Nat. Protoc. 6 (2011) 1355–1366.
[18] G. Zhang, G.M. Palmer, M.W. Dewhirst, C.L. Fraser, Nat. Mater. 8 (2009) 747–751.
[19] S. Zhang, M. Hosaka, T. Yoshihara, K. Negishi, Y. Iida, S. Tobita, T. Takeuchi, Cancer Res. 70 (2010), 4490-448.
[20] G.E. Arteel, R.G. Thurman, J.M. Yates, J.A. Raleigh, Br. J. Canc. 72 (1995) 889–895.
[21] M.W. Gross, U. Karbach, K. Groebe, A.J. Franko, W. Mueller-Klieser, Int. J. Canc. 61 (1995) 567–573.
[22] M.R. Horsman, L.S. Mortensen, J.B. Petersen, M. Busk, J. Overgaard, Nat. Rev. Clin. Oncol. 9 (2012) 674–687.
[23] M.M. Kleiter, D.E. Thrall, D.E. Malarkey, D.Y.W. Lee, S.C. Chou, J.A. Raleigh, Int. J. Radiat. Oncol. Biol. Phys. 64 (2006) 592–602.
[24] Y.G. Wang, K.J. Zhou, G. Huang, C. Hensley, X.N. Huang, X.P. Ma, T. Zhao, B.D. Sumer, R.J. DeBerardinis, J.M. Gao, Nat. Mater. 13 (2014) 204–212.
[25] Q. Zhao, F.Y. Li, C.H. Huang, Chem. Soc. Rev. 39 (2010) 3007–3030.
[26] K.Y. Zhang, Q. Yu, H. Wei, S.J. Liu, Q. Zhao, W. Huang, Chem. Rev. 118 (2018) 1170–1839.
[27] D.B. Papkovsky, R.I. Dmitriev, Chem. Soc. Rev. 42 (2013) 8700–8732.

[28] C.F. Wu, B. Bull, K. Christensen, J. McNeill, Angew. Chem. 121 (2009) 2779–2783. Angew. Chem. Int. Ed. 48 (2009) 2741-2745.
[29] T. Yoshihara, Y. Yamaguchi, M. Hosaka, T. Takeuchi, S. Tobita, Angew. Chem. Int. Ed. 51 (2012) 4148–4151.
[30] S.J. Zhang, M. Hosaka, T. Yoshihara, K. Negishi, Y. Iida, S. Tobita, T. Takeuchi, Cancer Res. 70 (2010) 4490–4498.
[31] T.C. Huang, X. Tong, Q. Yu, H.R. Yang, S. Guo, S.J. Liu, Q. Zhao, K.Y. Zhang, W. Huang, J. Mater. Chem. C. 4 (2016) 10638–10645.
[32] Q. Zhao, X.B. Zhou, T.Y. Cao, K.Y. Zhang, L.J. Yang, S.J. Liu, H. Liang, H.R. Yang, F.Y. Li, W. Huang, Chem. Sci. 6 (2015) 1825–1831.
[33] H.F. Shi, X. Ma, Q. Zhao, B. Liu, Q.Y. Qu, Z.F. An, Y.L. Zhao, W. Huang, Adv. Funct. Mater. 24 (2014) 4823–4830.
[34] W. Lv, T.S. Yang, Q. Yu, Q. Zhao, K.Y. Zhang, H. Liang, S.J. Liu, F.Y. Li, W. Huang, Adv. Sci. 2 (2015) 1500107.
[35] X.C. Zheng, X. Wang, H. Mao, W. Wu, B.R. Liu, X.Q. Jiang, Nat. Commun. 6 (2015) 5834–6834.
[36] I. Sanchez-Barragan, J.M. Costa-Fernandez, M. Valledor, J.C. Campo, A. Sanz-Medel, Trends Anal. Chem. 25 (2006) 958–967.
[37] R.I. Dmitriev, S.M. Borisov, H. Düssmann, S.W. Sun, B.J. Müller, J. Prehn, V.P. Baklaushev, I. Klimant, D.B. Papkovsky, ACS Nano 9 (2015) 5275–5288.
[38] D.B. Papkovsky, R.I. Dmitriev, Chem. Soc. Rev. 42 (2013) 8700–8732.
[39] X.L. Feng, L.B. Liu, S. Wang, D.B. Zhu, Chem. Soc. Rev. 39 (2010) 2411–2419.
[40] F.D. Feng, F. He, L.L. An, S. Wang, Adv. Mater. 20 (2008) 2959–2964.
[41] C.L. Zhu, L.B. Liu, Q. Yang, F.T. Lv, S. Wang, Chem. Rev. 112 (2012) 4687–4735.
[42] H. Jiang, P. Taranekar, J.R. Reynolds, K.S. Schanze, Angew. Chem. Int. Ed. 48 (2009) 4300–4316.
[43] A. Herland, O. Inganäs, Macromol. Rapid Commun. 28 (2007) 1703–1713.
[44] K. Lee, J. Lee, J.E. Jeong, A. Kronk, K.S.J. Elenitoba-Johnson, M.S. Lim, J. Kim, Adv. Mater. 24 (2012) 2479–2484.
[45] X.L. Feng, G.M. Yang, L.B. Liu, F.T. Lv, Q. Yang, S. Wang, D.B. Zhu, Adv. Mater. 24 (2012) 637–641.
[46] D. Hara, H. Komatsu, A. Son, S. Nishimoto, K. Tanabe, Bioconjug. Chem. 26 (2015) 645–649.